IEEE Access
Multidisciplinary ⋮ Rapid Review ⋮ Open Access Journal

Received July 29, 2019, accepted August 7, 2019, date of publication August 12, 2019, date of current version August 28, 2019.

Digital Object Identifier 10.1109/ACCESS.2019.2934404

Lyapunov Energy Function Based Control Method for Three-Phase UPS Inverters With Output Voltage Feedback Loops

SERTAC BAYHAN[1], (Senior Member, IEEE), S. SAJJAD SEYEDALIPOUR[2], HASAN KOMURCUGIL[3], (Senior Member, IEEE), AND HAITHAM ABU-RUB[4], (Fellow, IEEE)

[1]Qatar Environment and Energy Research Institute, Hamad Bin Khalifa University, Doha, Qatar
[2]Faculty of Electrical Engineering, K. N. Toosi University of Technology, Tehran, Iran
[3]Department of Computer Engineering, Eastern Mediterranean University, 10 Mersin, Turkey
[4]Department of Electrical and Computer Engineering, Texas A&M University at Qatar, Doha, Qatar

Corresponding author: Sertac Bayhan (sbayhan@hbku.edu.qa)

This work was supported by the Qatar National Library.

ABSTRACT In this study, a Lyapunov energy function based control method with output voltage feedback loops is proposed for three-phase uninterruptible power supply (UPS) inverters. The presented paper demonstrates that the traditional Lyapunov-energy-function-based control method not only leads to considerable steady-state error in the output voltage, but also distorts the output voltage waveforms. Therefore, a modification has been performed on the traditional Lyapunov-energy-function-based control by incorporating the output voltage feedback loops in the control variables. The robustness of the proposed control method has been studied analytically through transfer functions which are expressed as the ratio of the output voltage to its reference. These analytical results are validated experimentally. In addition, the steady-state and dynamic performances of the proposed control method are also tested experimentally on a three-phase UPS inverter operating with linear (resistive) and nonlinear (diode-bridge rectifier) loads. As a consequence of incorporating output voltage feedback loops into the control variables, the proposed control method offers strong robustness against variations in *LC* filter parameters, high-quality sinusoidal output voltage along with acceptable total harmonic distortion (THD) values under linear and nonlinear loads, fast dynamic response under abrupt load changes, and negligibly small steady-state error in the output voltage.

INDEX TERMS Uninterruptible power supply inverter, Lyapunov energy function, output voltage feedback, steady-state error, robustness.

I. INTRODUCTION

Critical loads such as communication systems, medical equipment and data centers are usually fed by uninterruptible power supply (UPS) systems in case of grid power failures [1], [2]. These loads need high quality power and reliable voltage at their input terminals regardless of voltage anomalies at the grid side. Therefore, a high-quality UPS system is required which should possess certain features such as rapid dynamic response regardless of load conditions, low total harmonic distortion (THD) in the load voltage, reasonably good tracking performance, guaranteed stability, and strong robustness against model mismatches and parameters variations.

In order to attain the aforementioned requirements, numerous control strategies have been reported for UPS inverters in the literature. The model predictive control (MPC) with load current observer offers a simple implementation, but the obtained results do not show a remarkable performance in terms of steady-state error and THD [3]–[5]. Moreover, MPC is dependent on the system parameters. Although the deadbeat (DB) control method exhibits rapid dynamic response, it is also dependent on the system parameters which may cause unstable operation when the system parameter variations are large [6], [7]. Even though the repetitive control technique removes the periodic disturbances effectively and provides satisfactory performance

The associate editor coordinating the review of this article and approving it for publication was Amin Hajizadeh.

in the steady-state operation, its dynamic response is slow and performance is not satisfactory under non-periodic disturbance conditions [8]–[12]. The H-infinity control method introduced in [13] offers satisfactory dynamic response. However, the output voltage is distorted under nonlinear load. The feedback linearization based control technique described in [14] achieves a satisfactory THD performance under nonlinear loads. However, the effect of parameter variations is not taken into consideration. Moreover, the implementation of the control approach is complicated. Although the flatness-based control in [15] achieves a satisfactory THD level and exhibits good dynamic response, its design is also complicated.

In addition to these control methods, various types of methodologies are also proposed for the UPS inverters. In [16], the adaptive voltage control along with low THD has been presented. The main drawback of this method is the risk of divergence if the gains are not appropriately chosen. Even though the high performance sinusoidal pulse width modulation based control approach introduced in [17] performs satisfactory in the steady-state under nonlinear loads, the load voltage is still distorted. The iterative learning control method achieves high performance under nonlinear loads at the expense of high switching frequency which leads to high switching losses [18]. The robust tracking control method proposed in [19] combines the features of deadbeat and robust control approaches which yield fast dynamic response as well as high robustness to model uncertainties. In [20], an observer-based optimal voltage control method is presented which involves two parts. While the first part ensures zero steady-state error, the other part is responsible for estimating the system uncertainties. The main problem of this method is that it involves too many gains with many possible values which make it difficult to select the optimal values for the desired performance. On the other hand, sliding mode control (SMC) methods are also emerged as possible solutions for controlling the UPS inverters [21]–[23]. Despite the fast dynamic response, robustness against system parameter variations and disturbances, and implementation simplicity, the SMC suffers from the time-varying switching frequency and chattering phenomenon. A discrete-time voltage control based on z-domain model is proposed in [24] where the computation and modulation delay can be precisely modeled. However, the results are not satisfactory.

The Lyapunov-energy-function-based control method offers good steady-state and fast dynamic responses in rectifier [25] and active filter applications [26]. However, there is no research investigating the applicability of Lyapunov-energy-function-based control method on three-phase UPS inverters. The idea of this control approach is based on finding a control law which makes the derivative of Lyapunov energy function always negative under all operating points. In such a case, the behavior of the closed-loop system around its equilibrium point can be analyzed. It is revealed that the traditional Lyapunov-energy-function-based control causes considerable steady-state error and large distortion in the output voltage. Thus, this method is modified by incorporating

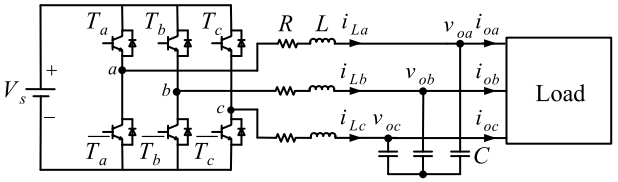

FIGURE 1. Three-phase UPS inverter with an output *LC* filter.

the output voltage feedback loops into the control variables. The proposed method reduces the steady-state error and improves the output voltage quality considerably. Additionally, d- and q- components transfer functions from reference output voltage to actual output voltage are derived in terms of the LC filter parameters. Then, a frequency domain study is performed to reveal that the proposed control strategy ensures the desired performance under parameters variations of the LC filter. The effectiveness of the proposed control method is investigated and compared with the results obtained from DB and SMC methods presented in [7] and [23] using a three-phase UPS inverter prototype.

II. THREE-PHASE INVERTER MODELING

A three-phase UPS inverter with an output LC filter is depicted in Fig. 1. The differential equations describing the inverter operation can be written in the abc frame as follows

$$\begin{aligned} L\frac{di_{La}}{dt} &= \frac{1}{2}u_a V_s - Ri_{La} - v_{oa} \\ L\frac{di_{Lb}}{dt} &= \frac{1}{2}u_b V_s - Ri_{Lb} - v_{ob} \\ L\frac{di_{Lc}}{dt} &= \frac{1}{2}u_c V_s - Ri_{Lc} - v_{oc} \end{aligned} \tag{1}$$

$$\begin{aligned} C\frac{dv_{oa}}{dt} &= i_{La} - i_{oa} \\ C\frac{dv_{ob}}{dt} &= i_{Lb} - i_{ob} \\ C\frac{dv_{oc}}{dt} &= i_{Lc} - i_{oc} \end{aligned} \tag{2}$$

In (1), u_a, u_b and u_c denote the control variables in the abc frame. In three-phase systems, it is quite reasonable to work in the synchronously rotating dq frame. Hence, equations (1) and (2) can be easily expressed in the synchronously rotating dq frame as follows

$$\begin{aligned} L\frac{di_{Ld}}{dt} &= \frac{1}{2}u_d V_s - Ri_{Ld} - v_{od} + \omega Li_{Lq} \\ L\frac{di_{Lq}}{dt} &= \frac{1}{2}u_q V_s - Ri_{Lq} - v_{oq} - \omega Li_{Ld} \end{aligned} \tag{3}$$

$$\begin{aligned} C\frac{dv_{od}}{dt} &= i_{Ld} - i_{od} + \omega Cv_{oq} \\ C\frac{dv_{oq}}{dt} &= i_{Lq} - i_{oq} - \omega Cv_{od} \end{aligned} \tag{4}$$

where u_d and u_q denote the control variables in the dq frame, ω is the angular frequency, R is the resistance of L. The control variables can be considered as the addition of steady-state

and perturbed terms shown below

$$u_d = U_d + \Delta u_d$$
$$u_q = U_q + \Delta u_q \tag{5}$$

where U_d and U_q are the steady-state terms, Δu_d and Δu_q are the perturbed terms of the control variables.

III. LYAPUNOV-ENERGY-FUNCTION-BASED CONTROL METHOD

The expressions of control variables in the steady-state can be solved from (3) by assuming that the actual variables track their reference variables in the steady-state ($i_{Ld} = i^*_{Ld}$, $i_{Lq} = i^*_{Lq}$, $v_{od} = v^*_{od}$, $v_{oq} = v^*_{oq}$, $u_d = U_d$, $u_q = U_q$) as follows

$$U_d = \frac{2}{V_s}\left(R' i^*_{Ld} + L' \frac{di^*_{Ld}}{dt} + v^*_{od} - \omega L' i^*_{Lq}\right)$$
$$U_q = \frac{2}{V_s}\left(R' i^*_{Lq} + L' \frac{di^*_{Lq}}{dt} + v^*_{oq} + \omega L' i^*_{Ld}\right) \tag{6}$$

where i^*_{Ld} and i^*_{Lq} are defined as

$$i^*_{Ld} = C' \frac{dv^*_{od}}{dt} + i_{od} - \omega C' v^*_{oq}$$
$$i^*_{Lq} = C' \frac{dv^*_{oq}}{dt} + i_{oq} + \omega C' v^*_{od} \tag{7}$$

Clearly, in order to be able to compute U_d and U_q in (6), the values of L and R are needed. However, it is not possible to know the exact values of these parameters in practice. Therefore, the estimated values of L and R, denoted by L' and R', are used in (6). The reference inductor currents i^*_{Ld} and i^*_{Lq} needed in (6) can be easily computed by using (7) which is dependent on v^*_{od}, v^*_{oq} and estimated value of C which is denoted by C'. Now, let us define the state variables and parameter mismatch errors as

$$x_1 = i_{Ld} - i^*_{Ld}, \quad x_2 = i_{Lq} - i^*_{Lq},$$
$$x_3 = v_{od} - v^*_{od}, \quad x_4 = v_{oq} - v^*_{oq} \tag{8}$$
$$\Delta R = R' - R, \quad \Delta L = L' - L, \quad \Delta C = C' - C \tag{9}$$

With the help of (8) and (9), equations (3) and (4) can be rewritten as

$$L\frac{dx_1}{dt} = \frac{1}{2}\Delta u_d V_s + \Delta L \frac{di^*_{Ld}}{dt} - Rx_1 + \Delta R i^*_{Ld} - x_3 + \omega L x_2 - \omega \Delta L i^*_{Lq}$$
$$L\frac{dx_2}{dt} = \frac{1}{2}\Delta u_q V_s + \Delta L \frac{di^*_{Lq}}{dt} - Rx_2 + \Delta R i^*_{Lq} - x_4 - \omega L x_1 + \omega \Delta L i^*_{Ld} \tag{10}$$
$$C\frac{dx_3}{dt} = \Delta C \frac{dv^*_{od}}{dt} + x_1 + \omega C x_4 - \omega \Delta C v^*_{oq}$$
$$C\frac{dx_4}{dt} = \Delta C \frac{dv^*_{oq}}{dt} + x_2 - \omega C x_3 + \omega \Delta C v^*_{od} \tag{11}$$

According to the Lyapunov-energy-function-based control approach, a linear or nonlinear system is asymptotically stable if the Lyapunov energy function $V(x)$ holds the following conditions: i) $V(0) = 0$, ii) $V(x) > 0$ for all $x \neq 0$, iii) $V(x) \to \infty$ as $\|x\| \to \infty$, and iv) $\frac{dV(x)}{dt} < 0$ for all $x \neq 0$. Even though the Kharitonov's theorem is also useful in assessing robust stability, knowledge of the coefficients in the characteristic equation is required within the specified range [27].

The expressions of Δu_d and Δu_q can be determined from the last condition. In Fig. 1, except for R and switching losses, there is no element that dissipates energy. The capacitor and inductor in LC filter store energy rather than dissipating it. When dc input voltage source V_s injects energy into the UPS inverter system, while some part of the injected energy is continuously transferred in the LC filter in bidirectional way, the rest of it is transferred to the load. The energy stored in L and C is in the form of $0.5Li_L^2$ for inductor and $0.5Cv_o^2$ for capacitor. Since the UPS inverter in Fig. 1 is modeled in the rotating dq frame, there are d- and q- components for inductor current and capacitor voltage. This implies that $V(x)$ should contain four terms as shown below

$$V(x) = \frac{3}{4}Lx_1^2 + \frac{3}{4}Lx_2^2 + \frac{3}{4}Cx_3^2 + \frac{3}{4}Cx_4^2 \tag{12}$$

It is evident that $V(x)$ satisfies first three conditions mentioned above. For the sake of satisfying the last condition, the derivative of (12) can be written as

$$\frac{dV(x)}{dt} = \frac{3}{2}L\frac{dx_1}{dt}x_1 + \frac{3}{2}L\frac{dx_2}{dt}x_2 + \frac{3}{2}C\frac{dx_3}{dt}x_3 + \frac{3}{2}C\frac{dx_4}{dt}x_4 \tag{13}$$

Replacing (10) and (11) into (13) results in

$$\begin{aligned}\frac{dV(x)}{dt} = {} & \frac{3}{2}x_1\Delta L\frac{di^*_{Ld}}{dt} + \frac{3}{2}x_1\Delta R i^*_{Ld} - \frac{3}{2}x_1\omega\Delta L i^*_{Lq} \\ & + \frac{3}{2}x_2\Delta L\frac{di^*_{Lq}}{dt} + \frac{3}{2}x_2\Delta R i^*_{Lq} + \frac{3}{2}x_2\omega\Delta L i^*_{Ld} \\ & + \frac{3}{2}x_3\Delta C\frac{dv^*_{od}}{dt} - \frac{3}{2}x_3\omega\Delta C v^*_{oq} + \frac{3}{2}x_4\Delta C\frac{dv^*_{oq}}{dt} \\ & + \frac{3}{2}x_4\omega\Delta C v^*_{od} - \frac{3}{2}Rx_1^2 - \frac{3}{2}Rx_2^2 + \frac{3}{4}x_1\Delta u_d V_s \\ & + \frac{3}{4}x_2\Delta u_q V_s\end{aligned} \tag{14}$$

When the actual and estimated parameters are equal ($\Delta R = \Delta L = \Delta C = 0$), $dV(x)/dt$ is always negative if Δu_d and Δu_q are defined as

$$\Delta u_d = K_{id} V_s x_1$$
$$\Delta u_q = K_{iq} V_s x_2 \tag{15}$$

where $K_{id} < 0$ and $K_{iq} < 0$ are negative real constants. Hence, the general expressions of u_d and u_q become

$$u_d = \frac{2}{V_s}\left(R' i^*_{Ld} + L' \frac{di^*_{Ld}}{dt} + v^*_{od} - \omega L' i^*_{Lq}\right) + K_{id} V_s x_1$$
$$u_q = \frac{2}{V_s}\left(R' i^*_{Lq} + L' \frac{di^*_{Lq}}{dt} + v^*_{oq} + \omega L' i^*_{Ld}\right) + K_{iq} V_s x_2 \tag{16}$$

Equation (16) is the traditional Lyapunov-function-based controller which achieves the control of v_o indirectly provided that i_{Ld} and i_{Lq} track their references [25]. Otherwise, there exists steady-state error in v_o.

In order to alleviate the steady-state error in v_o, Δu_d and Δu_q in (15) are modified by adding x_3 and x_4 (output voltage feedback loops) as

$$\begin{aligned}\Delta u_d &= K_{id}V_s x_1 - K_{vd}x_3\\ \Delta u_q &= K_{iq}V_s x_2 - K_{vq}x_4\end{aligned} \tag{17}$$

Substituting (17) into (14) yields

$$\begin{aligned}\frac{dV(x)}{dt} &= \frac{3}{2}x_1\Delta L\frac{di^*_{Ld}}{dt} + \frac{3}{2}x_1\Delta R i^*_{Ld} - \frac{3}{2}x_1\omega\Delta L i^*_{Lq}\\ &+ \frac{3}{2}x_2\Delta L\frac{di^*_{Lq}}{dt} + \frac{3}{2}x_2\Delta R i^*_{Lq} + \frac{3}{2}x_2\omega\Delta L i^*_{Ld}\\ &+ \frac{3}{2}x_3\Delta C\frac{dv^*_{od}}{dt} - \frac{3}{2}x_3\omega\Delta C v^*_{oq} + \frac{3}{2}x_4\Delta C\frac{dv^*_{oq}}{dt}\\ &+ \frac{3}{2}x_4\omega\Delta C v^*_{od} - \frac{3}{2}Rx_1^2 - \frac{3}{2}Rx_2^2 + \frac{3}{4}K_{id}V_s^2x_1^2\\ &+ \frac{3}{4}K_{iq}V_s^2x_2^2 - \frac{3}{4}K_{vd}V_s x_3 x_1 - \frac{3}{4}K_{vq}V_s x_4 x_2\end{aligned} \tag{18}$$

The terms which involve ΔR, ΔL and ΔC have considerably smaller impact on the negative definiteness of $dV(x)/dt$. Hence, setting ΔR, ΔL and ΔC to zero in (18) does not deteriorate the idea behind Lyapunov-function-based approach (in the next section, it will be shown that the system stability is not affected by the filter parameter variations). In this case, the overall expressions of u_d and u_q are written as

$$\begin{aligned}u_d &= \frac{2}{V_s}\left(R'i^*_{Ld} + L'\frac{di^*_{Ld}}{dt} + v^*_{od} - \omega L' i^*_{Lq}\right) + K_{id}V_s x_1\\ &- K_{vd}x_3\\ u_q &= \frac{2}{V_s}\left(R'i^*_{Lq} + L'\frac{di^*_{Lq}}{dt} + v^*_{oq} + \omega L' i^*_{Ld}\right) + K_{iq}V_s x_2\\ &- K_{vq}x_4\end{aligned} \tag{19}$$

In order to investigate the influence of neglecting the parameter variations on the negative definiteness of $dV(x)/dt$, the closed-loop system has been simulated using the control law in equation (19) with +30% parameter variations and without parameter variations under resistive load. Fig. 2 shows the responses of $dV(x)/dt$ obtained with +30% parameter mismatch and without parameter mismatch in one period.

Clearly, $dV(x)/dt$ remains negative with and without parameter variations as shown in Fig. 2. The block diagram of the proposed Lyapunov-energy-function-based control method with output voltage feedback loops is depicted in Fig. 3.

IV. INVESTIGATION ON ROBUSTNESS

In this section, the effect of LC filter variations on the performance of the proposed control method is investigated.

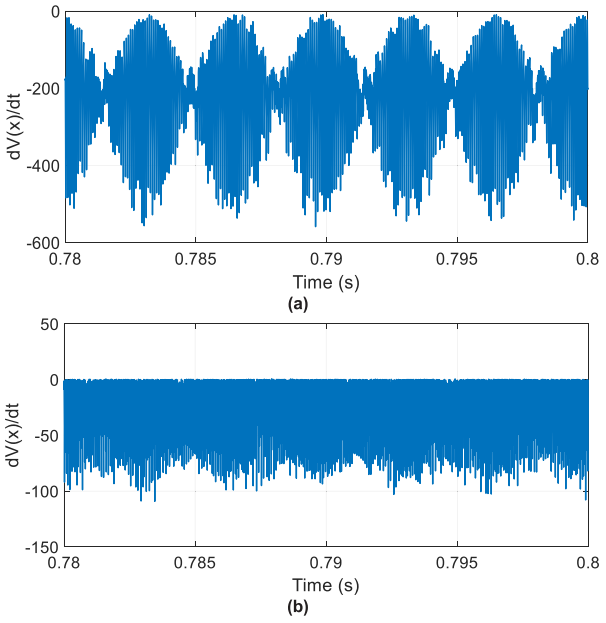

FIGURE 2. Responses of $dV(x)/dt$ in one period with and without parameter variations. (a) +30% parameter mismatch, (b) Perfect match.

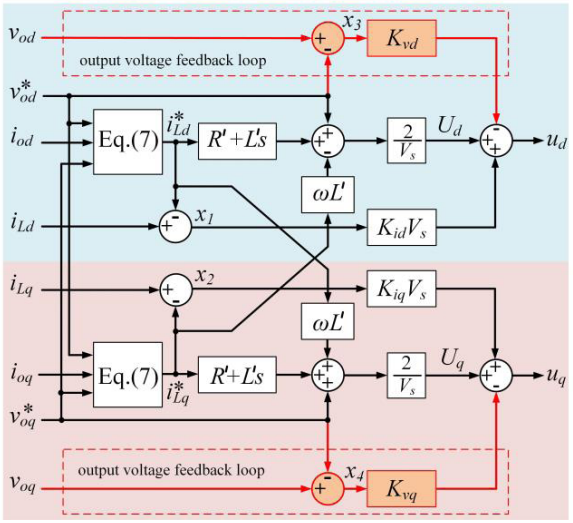

FIGURE 3. Block diagram of the proposed Lyapunov-energy-function-based control method with output voltage feedback loops.

Substitution of (19) into (3) yields

$$\begin{aligned}&L\frac{di_{Ld}}{dt}\\ &= L'\frac{di^*_{Ld}}{dt} - Ri_{Ld} + R'i^*_{Ld} + \frac{1}{2}K_{id}V_s^2\left(i_{Ld} - i^*_{Ld}\right)\\ &\quad - \frac{1}{2}V_sK_{vd}\left(v_{od} - v^*_{od}\right) - v_{od} + v^*_{od} + \omega L i_{Lq} - \omega L' i^*_{Lq}\\ &L\frac{di_{Lq}}{dt}\\ &= L'\frac{di^*_{Lq}}{dt} - Ri_{Lq} + R'i^*_{Lq} + \frac{1}{2}K_{iq}V_s^2\left(i_{Lq} - i^*_{Lq}\right)\\ &\quad - \frac{1}{2}V_sK_{vq}\left(v_{oq} - v^*_{oq}\right) - v_{oq} + v^*_{oq} - \omega L i_{Ld} + \omega L' i^*_{Ld}\end{aligned} \tag{20}$$

For the sake of simplifying the analysis, we consider

$$\begin{aligned} K_{id} &= K_{iq} = 2\alpha \\ K_{vd} &= K_{vq} = 2\beta \end{aligned} \tag{21}$$

The d- and q- components of output voltage in Laplace domain can be written in terms of the transfer functions as follows

$$\begin{aligned} V_{od}(s) &= G_1(s) V_{od}^*(s) + G_2(s) I_{od}(s) + G_3(s) I_{oq}(s) \\ V_{oq}(s) &= G_1'(s) V_{od}^*(s) + G_2'(s) I_{od}(s) + G_3'(s) I_{oq}(s) \end{aligned} \tag{22}$$

where the transfer functions are given by

$$G_1(s) = \frac{A(s)}{D(s)}, \quad G_2(s) = \frac{B(s)}{D(s)}, \; G_3(s) = \frac{C(s)}{D(s)}$$
$$G_1'(s) = \frac{A'(s)}{D(s)}, \quad G_2'(s) = \frac{B'(s)}{D(s)}, \; G_3'(s) = \frac{C'(s)}{D(s)}$$

and the polynomials $A(s)$, $A'(s)$, $B(s)$, $B'(s)$, $C(s)$, $C'(s)$ and $D(s)$ are in the form of $X(s) = X_4 s^4 + X_3 s^3 + X_2 s^2 + X_1 s + X_0$ whose coefficients are defined as

$$\begin{aligned} A_4 &= LL'CC' \\ A_3 &= \left(R' - \alpha V_s^2\right) LCC' + \left(R - \alpha V_s^2\right) L'C'C \\ A_2 &= CC' \left(R' - \alpha V_s^2\right) \left(R - \alpha V_s^2\right) + 4\omega^2 LL'CC' \\ &\quad + \left(\beta V_s + 1 - \omega^2 LC\right) L'C' + \left(\beta V_s + 1 - \omega^2 L'C'\right) LC \\ A_1 &= C' \left(R' - \alpha V_s^2\right) \left(\beta V_s + 1 - \omega^2 LC\right) \\ &\quad + C \left(R - \alpha V_s^2\right) \left(\beta V_s + 1 - \omega^2 L'C'\right) \\ &\quad + 2\omega^2 LCC' \left(R' - \alpha V_s^2\right) + 2\omega^2 L'CC' \left(R - \alpha V_s^2\right) \\ A_0 &= \left(\beta V_s + 1 - \omega^2 LC\right) \left(\beta V_s + 1 - \omega^2 L'C'\right) \\ &\quad + \omega^2 CC' \left(R' - \alpha V_s^2\right) \left(R - \alpha V_s^2\right) \\ B_3 &= LC\Delta L \\ B_2 &= LC\Delta R + C\Delta L \left(R - \alpha V_s^2\right) \\ B_1 &= C\Delta R \left(R - \alpha V_s^2\right) + \Delta L \left(\beta V_s + 1 + \omega^2 LC\right) \\ B_0 &= \Delta R \left(\beta V_s + 1 - \omega^2 LC\right) + \omega^2 C\Delta L \left(R - \alpha V_s^2\right) \\ C_2 &= \omega LC\Delta L \\ C_1 &= 2\omega LC\Delta R \\ C_0 &= \omega C\Delta R \left(R - \alpha V_s^2\right) - \omega\Delta L \left(\beta V_s + 1 - \omega^2 LC\right) \\ A_2' &= \omega L'CC' \left(R - \alpha V_s^2\right) - \omega LCC' \left(R' - \alpha V_s^2\right) \\ A_1' &= 2\omega \left(\beta V_s + 1\right) \left(L'C' - LC\right) \\ A_0' &= \omega C' \left(R' - \alpha V_s^2\right) \left(\beta V_s + 1 - \omega^2 LC\right) \\ &\quad - \omega C \left(R - \alpha V_s^2\right) \left(\beta V_s + 1 - \omega^2 L'C'\right) \\ B'(s) &= -C(s) \\ C'(s) &= B(s) \\ D_4 &= L^2C^2 \\ D_3 &= 2LC^2 \left(R - \alpha V_s^2\right) \\ D_2 &= 2LC \left(\beta V_s + 1 + \omega^2 LC\right) + C^2 \left(R - \alpha V_s^2\right)^2 \\ D_1 &= 2C \left(R - \alpha V_s^2\right) \left(\beta V_s + 1 + \omega^2 LC\right) \\ D_0 &= \omega^2 C^2 \left(R - \alpha V_s^2\right)^2 + \left(\beta V_s + 1 - \omega^2 LC\right)^2 \end{aligned}$$

In order to simplify the analysis, v_{oq}^* is considered to be zero. The characteristic equation of the closed-loop system is the denominator of the transfer functions defined as

$$D_4 s^4 + D_3 s^3 + D_2 s^2 + D_1 s + D_0 \tag{23}$$

Close inspection of (23) provides an insight into the fact that the characteristic equation is not dependent on ΔR, ΔL and ΔC. In other words, the closed-loop system stability is not influenced from the variations in the LC filter parameters. From Routh–Hurwitz stability criterion, the poles of the closed-loop system can be located in the left half plane if the following inequalities hold

$$D_4,\; D_3,\; D_2,\; D_1,\; D_0 > 0 \tag{24}$$
$$D_3 D_2 - D_4 D_1 > 0 \tag{25}$$
$$D_3 D_2 D_1 - D_4 D_1^2 - D_3^2 D_0 > 0 \tag{26}$$

The condition in (24) can be satisfied if $\alpha < 0$ and $\beta > -\frac{1+\omega^2 LC}{V_s}$. Also, irrespective of the system parameters, (25) and (26) are always satisfied.

The root locus of poles, plotted using the system parameters given in Section V by varying α in the interval $[-0.00001, -0.001]$ while β is maintained at 0 (output voltage loops are disabled) and 0.125 (output voltage loops are activated), is shown in Figs. 4(a) and 4(b), respectively. With the initial values of α and β($\beta = 0$ and $\beta = 0.125$), the poles are complex conjugate pairs with the imaginary components much larger than the real components and are located in the left half plane very close to the imaginary axis. However, when the value of $|\alpha|$ is increased while β is kept unchanged, the pole pairs move away from the imaginary axis toward the negative real axis with an elliptical trajectory for both β values. Comparing the poles on the elliptical trajectories in Figs. 4(a) and 4(b), one can see that the poles in Fig. 4(b) have much larger magnitudes (real and imaginary) than that of the poles in Fig. 4(a). For each β value ($\beta = 0$ and $\beta = 0.125$), it can be seen that there exists an α value which equates two poles at points K, M, N and O. The real parts of the poles are much larger than the imaginary parts at these points. Comparing the real parts of the poles obtained with the unique α value in Figs. 4(a) and 4(b), one can see that the real parts of the poles in Fig. 4(b) are greater than that presented in Fig. 4(a). This means that the closed-loop system with $\beta \neq 0$ is always faster than the closed-loop system with $\beta = 0$. When the value of $|\alpha|$ is increased further,

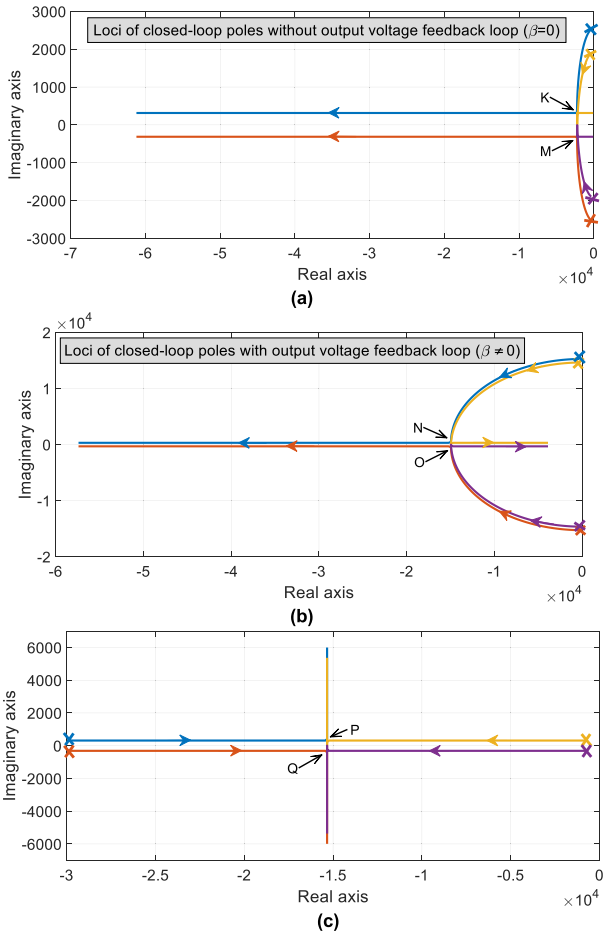

FIGURE 4. The loci of closed-loop poles obtained when (a) α is varied with $\beta = 0$, (b) α is varied with $\beta = 0.125$, (c) β is varied with $\alpha = -0.0005$.

the imaginary parts become very small, one of the pairs of poles continue moving away from the imaginary axis while other pair changes direction and moves toward the imaginary axis. On the other hand, the loci of the poles obtained by varying β in the interval [0.01, 0.15] while α is maintained at -0.0005 is shown in Fig. 4(c).

When β is increased gradually, the poles on left hand side move toward right and the poles on the right hand side move toward left until they reach points P and Q where two of the pole magnitudes are equal. Thereafter, any increment in β moves the equated poles up and down with no change in their real parts. In this case, the dynamic response is not affected by β. On the other hand, it is obvious from (22) that $G_1(s) = 1$ and $G_2(s) = G_3(s) = G_1'(s) = G_2'(s) = G_3'(s) = 0$ when $R' = R$, $L' = L$ and $C' = C$. This means that v_o tracks v_o^* with zero steady-state error when the estimated parameters are equal to the actual parameters. However, as mentioned before, such equality is not achievable in practice. For this reason, it is significant to assess the robustness of the Lyapunov-energy-function-based control methods.

A. ROBUSTNESS OF TRADITIONAL LYAPUNOV-ENERGY-FUNCTION-BASED CONTROL METHOD FOR RESISTIVE LOAD

The transfer functions in (22) represent traditional Lyapunov-function-based control for $\beta = 0$. Hence, substituting $I_{od}(s) = V_{od}(s)/R_l$ and $I_{oq}(s) = V_{oq}(s)/R_l$ into (22) gives

$$H(s) = \frac{V_{od}(s)}{V_{od}^*(s)} = \frac{G_1(s)\left(1 - \frac{G_2(s)}{R_l}\right) + \frac{G_1'(s)G_3(s)}{R_l}}{\left(1 - \frac{G_2(s)}{R_l}\right)^2 + \left(\frac{G_3(s)}{R_l}\right)^2} \quad (27)$$

$$H'(s) = \frac{V_{oq}(s)}{V_{od}^*(s)} = \frac{G_1'(s)\left(1 - \frac{G_2(s)}{R_l}\right) - \frac{G_1(s)G_3(s)}{R_l}}{\left(1 - \frac{G_2(s)}{R_l}\right)^2 + \left(\frac{G_3(s)}{R_l}\right)^2} \quad (28)$$

where R_l denotes the load resistance. On the other hand, the steady-state output voltage in the frequency domain (replacing s with $j\omega$) can be written as

$$\begin{aligned} V_o(j\omega) &= V_{od}(j\omega) + jV_{oq}(j\omega) \\ &= H(j\omega)V_{od}^*(j\omega) + jH'(j\omega)V_{od}^*(j\omega) \end{aligned} \quad (29)$$

The output voltages in the steady-state are given by

$$\begin{aligned} v_{oa}(t) &= V_m \cos(\omega t + \phi) \\ v_{ob}(t) &= V_m \cos(\omega t - 2\pi/3 + \phi) \\ v_{oc}(t) &= V_m \cos(\omega t + 2\pi/3 + \phi) \end{aligned} \quad (30)$$

The amplitude and phase shift of the output voltage can be obtained as

$$\begin{aligned} V_m &= V_m^* \sqrt{\begin{array}{l}[|H(j\omega)|cos(\angle H(j\omega)) - |H'(j\omega)|\sin(\angle H'(j\omega))]^2 \\ +[|H(j\omega)|sin(\angle H(j\omega)) + |H'(j\omega)|\cos(\angle H'(j\omega))]^2\end{array}} \\ \phi &= \tan^{-1}\left(\frac{|H(j\omega)|\sin(\angle H(j\omega)) + |H'(j\omega)|cos(\angle H'(j\omega))}{|H(j\omega)|\cos(\angle H(j\omega)) - |H'(j\omega)|sin(\angle H'(j\omega))}\right) \end{aligned} \quad (31)$$

where V_m^* is the amplitude of the reference output voltage.

Fig. 5 shows the influence of parameter mismatch on v_o when the output voltage feedback loops are disabled ($K_{vd} = K_{vq} = 0$). The negative maximum amplitude error and phase shift (-3.36 Vrms and $-6.85°$) and the positive maximum amplitude error and phase shift (4.21 Vrms and 6.65°) occur in the case of -30 and $+30\%$ mismatches in R', L' and C'. For $+30\%$ parameter mismatch in R', L' and C', the output voltage tracking error ($e_v\% = (V_m - V_m^*)/V_m^* \times 100$) is 3.51% which is admissible according to the IEC62040-3 standard. As a consequence, with $\pm 30\%$ parameter mismatch, the amount of the steady-state error in v_o is low which means that the traditional Lyapunov-energy-function-based control method has reasonable robustness against parameter variations in LC. Although such robustness is authentic under ideal operating conditions, the steady-state error in v_o becomes larger in practice.

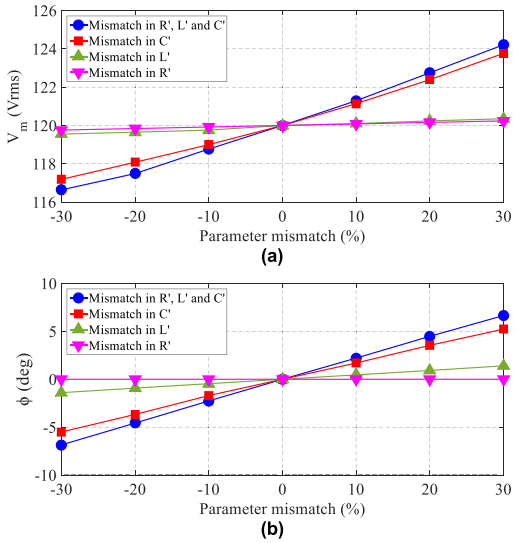

FIGURE 5. Influence of parameter mismatch on: (a) V_m and (b) ϕ when the output voltage feedback loops are disabled.

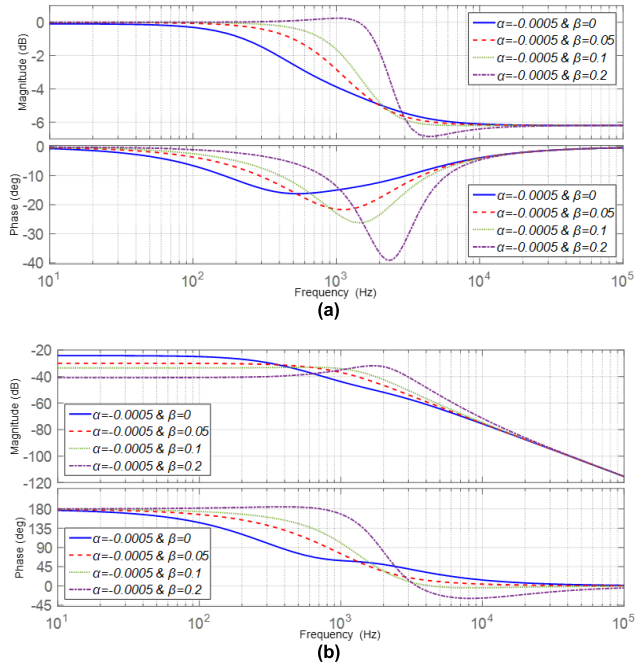

FIGURE 6. Magnitude and phase responses with −30% parameter mismatch. (a) $H(s)$, (b) $H'(s)$.

B. ROBUSTNESS OF PROPOSED LYAPUNOV-ENERGY-FUNCTION-BASED CONTROL METHOD FOR RESISTIVE LOAD

Fig. 6 depicts the magnitude and phase responses of $H(s)$ and $H'(s)$ obtained with −30% variations in LC filter parameters using a fixed value of α and different values of β. It can be seen that the magnitude response of $H(s)$ is not zero dB ($H(s) \neq 1$) for $\beta = 0$ leading to a steady-state error in v_o. However, when the output voltage feedback loops are activated, it is possible to achieve zero steady-state error in v_o by tuning β.

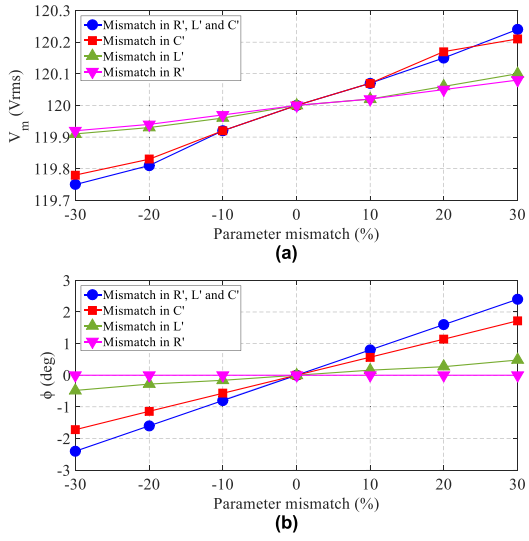

FIGURE 7. Influence of parameter mismatch on: (a) V_m and (b) ϕ when the output voltage feedback loops are active.

On the other hand, the magnitude response of $H'(s)$ is negative since $V_{oq}(s)$ is not zero due to −30% parameter mismatch. Fig. 7 shows the influence of parameter mismatch on v_o when the output voltage feedback loops are activated. It is clear from Fig. 5 and Fig. 7 that the steady-state error in v_o and ϕ are reduced considerably. For example, with +30% parameter mismatch in R', L' and C', the output voltage tracking error becomes 0.2% which is far from standard limitations. Hence, it can be concluded that the Lyapunov-energy-function-based control with output voltage feedback loop offers stronger robustness than the traditional Lyapunov-energy-function-based control method.

C. ROBUSTNESS OF PROPOSED LYAPUNOV-ENERGY-FUNCTION-BASED CONTROL METHOD FOR ANY LOAD

It is worth noting that it is very complicated to achieve analytical results for the output voltage when the UPS inverter supplies energy to a nonlinear load. For this reason, sub-section B is extended to include the operation of inverter under any load. Consequently, the effect of parameter mismatch on v_o can be evaluated by considering the transfer functions in the frequency domain. The numerators and denominator of the transfer functions are obtained in the frequency domain as follows

$$\begin{aligned} A(j\omega) &= (\beta V_s + 1)\left[\beta V_s + 1 - 2\omega^2\left(L'C' + LC\right)\right] \\ &\quad + j(\beta V_s + 1)\left[\omega C'\left(R' - \alpha V_s^2\right) + \omega C\left(R - \alpha V_s^2\right)\right] \\ B(j\omega) &= \Delta R\left(\beta V_s + 1 - 2\omega^2 LC\right) \\ &\quad + j\left[\omega C \Delta R\left(R - \alpha V_s^2\right) + \omega \Delta L(\beta V_s + 1)\right] \\ C(j\omega) &= \omega C \Delta R\left(R - \alpha V_s^2\right) - \omega \Delta L(\beta V_s + 1) + j2\omega^2 LC \Delta R \end{aligned}$$

$$
\begin{aligned}
A'(j\omega) &= \omega(\beta V_s + 1)\left[C'\left(R' - \alpha V_s^2\right) - C\left(R - \alpha V_s^2\right)\right] \\
&\quad + j2\omega^2(\beta V_s + 1)\left(L'C' - LC\right) \\
B'(j\omega) &= -C(j\omega) \\
C'(j\omega) &= B(j\omega) \\
D(j\omega) &= (\beta V_s + 1)\left(\beta V_s + 1 - 4\omega^2 LC\right) \\
&\quad + j2\omega C(\beta V_s + 1)\left(R - \alpha V_s^2\right)
\end{aligned}
$$

Ideally, $G_1(j\omega)$ must converge to unity and the other transfer functions converge to zero at the fundamental frequency. Considering the condition $\omega^2 LC << 1$ in above equations, it can be shown that $G_1(j\omega)$ converges to 1, and $G_2(j\omega)$, $G_3(j\omega)$, $G_1'(j\omega)$, $G_2'(j\omega)$, $G_3'(j\omega)$ converge to 0 for $\beta > 0$.

V. EXPERIMENTAL RESULTS

The performance of the proposed Lyapunov-function-based control method is evaluated experimentally on a three-phase UPS inverter prototype controlled by an OPAL-RT. The system parameters used in the experimental study are $V_s = 350\text{V}$, $V_m^* = 120\text{Vrms}$, $\omega = 100\pi$ rad/s, $R = 0.1\,\Omega$, and $f_{sw} = 12\text{kHz}$. The output filter is designed using the method presented in [28] as follows

$$
L = \frac{V_s}{8 f_{sw} i_{o,rated} \times \%ripple}, \quad C = \frac{\%ripple \times Q_{rated}}{\omega V_m^2} \tag{32}
$$

Substituting the values of V_s, f_{sw}, ω and V_m together with $i_{o,rated} = 20\text{A}$, $\%ripple = 10$, and $Q_{rated} = 5\text{kW}$ into (32) results in $L = 1.8\text{mH}$ and $C = 110\mu\text{F}$. Based on the availability of these components and considering $\pm\%10$ uncertainty, they were selected as $L = 2\text{mH}$, $C = 100\mu\text{F}$. The control parameters were selected such that the poles are located at points N and O shown in Fig. 4(b). The values of control parameters are determined to be $K_{id} = K_{iq} = 2\alpha = -0.001$ and $K_{vd} = K_{vq} = 2\beta = 0.25$.

Fig. 8 shows the steady-state responses of output voltages (*abc*, *dq* and $\alpha\beta$ frames), load currents (*abc* and $\alpha\beta$ frames) and spectrum of output voltages obtained with -30% parameter mismatch when the output voltage loops are disabled. The steady-state errors are discernible in the results obtained in the *dq* frame. In addition, the output voltages are distorted where the THD is measured as 8.7% as shown in Fig. 8(b). This distortion can be clearly seen in the $\alpha\beta$ frame shown in Fig. 8(c) where the load voltage and current components (horizontal axis: α-component, vertical axis: β-component) exhibit a distorted circle trajectory.

Fig. 9 shows the steady-state responses of output voltages (*abc*, *dq* and $\alpha\beta$ frames) and load currents (*abc* and $\alpha\beta$ frames) under 5kW resistive load obtained with -30% parameter mismatch when the output voltage loops are activated. It is obvious from Fig. 9(a) that the output voltages are sinusoidal. This fact is verified in the $\alpha\beta$ frame shown in Fig. 9(b) where the load voltage and current components exhibit circle trajectory. Comparing Figs. 8(a) and 9(a), one can see that the performance of the controller is much better when the output voltage loops are activated. Despite -30% parameter mismatch, v_{od} and v_{oq} are not distorted and they track their references with no steady-state error. These results verify the validity of the theoretical robustness study in section IV.

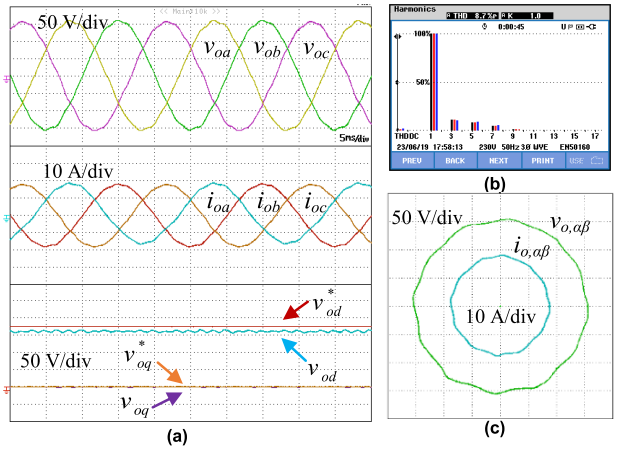

FIGURE 8. Steady-state responses of output voltages (*abc*, *dq* and $\alpha\beta$ frames), load currents (*abc* and $\alpha\beta$ frames) and harmonic spectrum of output voltages obtained with -30% parameter mismatch when the output voltage loops are disabled ($K_{vd} = K_{vq} = 0$, $K_{id} = K_{iq} = -0.001$). (a) *abc* and *dq* frames, (b) harmonic spectrum, (c) $\alpha\beta$ frame.

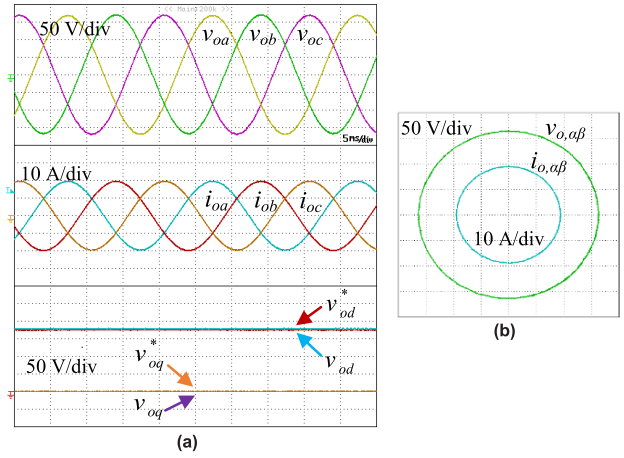

FIGURE 9. Steady-state responses of output voltages (*abc*, *dq* and $\alpha\beta$ frames) and load currents (*abc* and $\alpha\beta$ frames) under 5kW resistive load obtained with -30% parameter mismatch when output voltage loops are activated ($K_{vd} = K_{vq} = 0.25$, $K_{id} = K_{iq} = -0.001$). (a) *abc* and *dq* frames, (b) $\alpha\beta$ frame.

Fig. 10 shows the steady-state responses of output voltages and load currents under 5kW resistive load obtained with -30% parameter mismatch when the output voltage loops are activated and the current loop gains are set to $K_{id} = K_{iq} = -0.00002$. In spite of activating the output voltage loops, undesired oscillations occur on the output voltage waveforms due to the poles located very close to the imaginary axis as shown in Fig. 4(b).

Fig. 11 shows the dynamic responses of output voltages and load currents for an abrupt change in the resistive load from 2.5kW to 5kW obtained when the output voltage loops are activated and the parameter match is perfect.

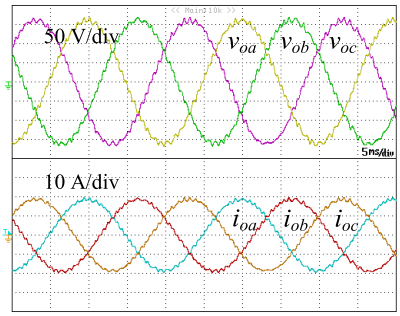

FIGURE 10. Steady-state responses of output voltages and load currents under 5kW resistive load obtained with −30% parameter mismatch when output voltage loops are activated and current loop gains are set to $K_{id} = K_{iq} = -0.00002$.

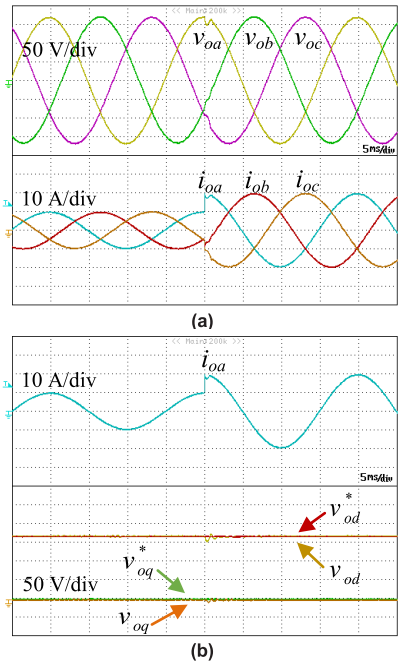

FIGURE 11. Dynamic responses of output voltages and load currents for an abrupt change in resistive load from 2.5kW to 5kW obtained when output voltage loops are activated. (a) Output voltages and currents, (b) Phase-*a* load current and actual and reference output voltages in the *dq* frame.

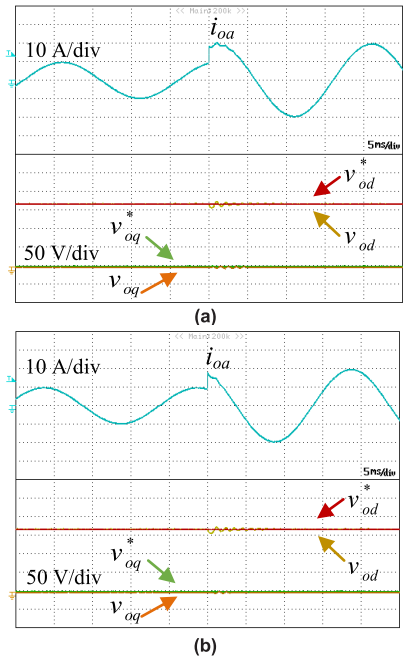

FIGURE 12. Dynamic responses of output voltages in the dq frame and phase-*a* load current for an abrupt change in resistive load from 2.5kW to 5kW when parameters in the control variables deviate (a) +30%, (b) −30%.

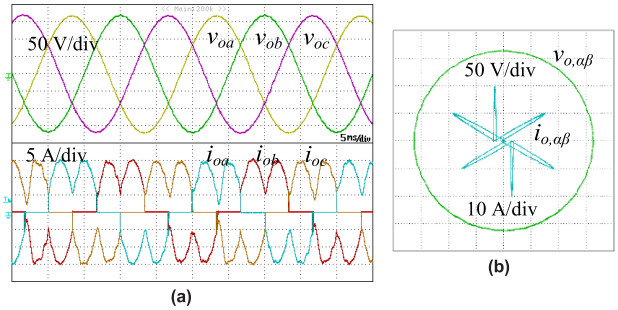

FIGURE 13. Steady-state responses of output voltages and load currents under nonlinear load in the *abc* and $\alpha\beta$ frames obtained with −30% parameter mismatch when output voltage loops are activated. (a) Output voltage and current waveforms in the *abc* frame, (b) Output voltage and current trajectories in the $\alpha\beta$ frame.

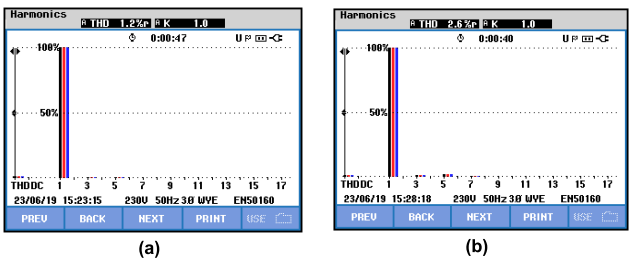

FIGURE 14. Harmonic spectrums of the output voltage under linear and nonlinear loads corresponding to Figs. 9 and 13.

Despite %100 of load change, the controller recovers the output voltage very fast. Compared to Fig. 8(a), v_{od} and v_{oq} track their references with zero steady-state error.

Fig. 12 shows the dynamic responses of the output voltages in the *dq* frame and phase-*a* load current for an abrupt change in the resistive load from 2.5kW to 5kW obtained with the proposed control method with output voltage loops activated when the parameters in the control variables deviate ±30% from the actual parameters.

The effects of parameter variations on the tracking capability of the proposed control method can be seen in Fig. 12(a) and 12(b) for +30% and −30%, respectively. Clearly, the actual voltage components (v_{od} and v_{oq}) track their references (v^*_{od} and v^*_{oq}) in both cases. This means that the proposed control method is robust against variations in the *LC* filter.

Fig. 13 shows the steady-state responses of the three-phase output voltages and load currents under nonlinear load (diode bridge rectifier with *RC* load) in the *abc* and $\alpha\beta$ frames

TABLE 1. Comparisons of five control methods with the proposed control method.

Comparison Category	[7]	[16]	[19]	[20]	[23]	Proposed control
DC link voltage (V)	390	600	450	290	390	350
Output voltage (V_rms)	110	220	110	110	110	120
Number of required sensors	9	6	6	6	6	6
Switching frequency (kHz)	12	4	10	5	15	12
Number of controller gains	0	Too many	4	Too many	6	4
Effect of variations in LC filter	Not reported	Not reported	Not reported	Not reported	Not reported	Negligible
Quality of v_o under nonlinear load	Distorted	Good	Distorted	Good	Distorted	Good
Steady-state error in v_o	Exists	Exists	Zero	Negligible	Exists	Negligible

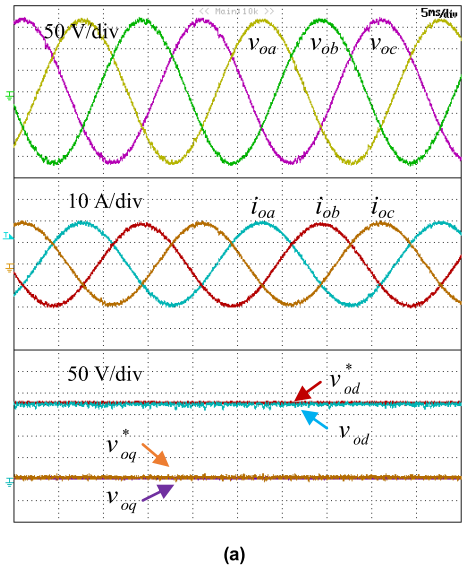

(a)

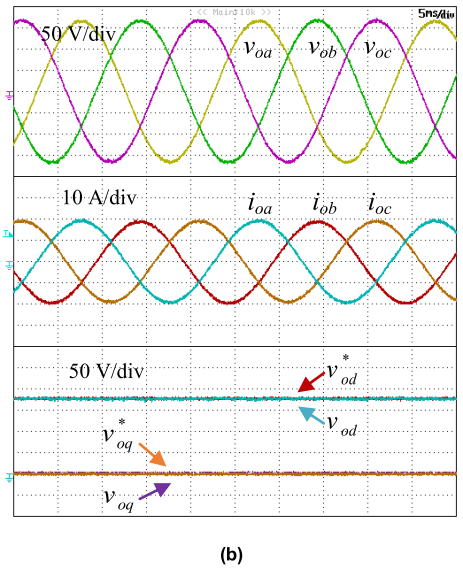

(b)

FIGURE 15. Steady-state responses of output voltages (*abc* and *dq* frames) and load currents (*abc* frame) under 5kW resistive load in case of −30% parameter mismatch obtained with: (a) DB control, (b) SMC.

obtained with −30% parameter mismatch when the output voltage loops are activated. Clearly, the output voltages are sinusoidal with negligible distortion. The load voltage ($v_{o,\,\alpha\beta}$) and load current ($i_{o,\,\alpha\beta}$) trajectories in the $\alpha\beta$ frame are shown

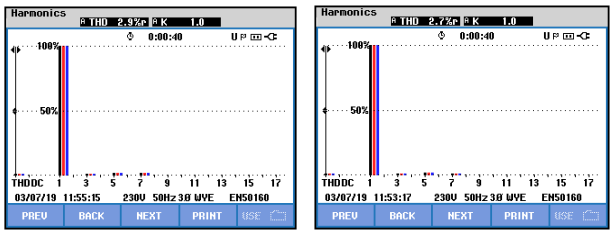

(a) (b)

FIGURE 16. Harmonic spectrums of the output voltage under linear load obtained with: (a) DB control, (b) SMC.

in Fig. 13(b). Circle trajectory of the load voltage verifies that the output voltages are sinusoidal and are almost not distorted with this highly nonlinear load.

Fig. 14 shows the harmonic spectrums together with the THD values of the output voltage under linear and nonlinear load cases corresponding to Figs. 9 and 13. The measured THDs are 1.2% and 2.6%, respectively. The 3^{rd}, 5^{th}, and 7^{th} harmonic components are very small.

The proposed control method is compared with the existing control methods presented in [7], [16], [19], [20], and [23] in terms of dc voltage input value, number of required sensors, switching frequency, number of controller gains, robustness to variations in LC filter, output voltage quality and steady-state error in the output voltage. It is apparent from Table 1 that the proposed method offers some important advantages over the existing ones in terms of achieving high robustness to variations in the LC filter, almost no steady-state error in the output voltage, good output voltage quality under nonlinear load, and the number of controller gains.

The measured steady-state error and THD values of the output voltage under linear and nonlinear load types obtained with and without voltage feedback loop using various parameter mismatch amounts are shown in Table 2. The steady-state error and THD values are reduced considerably when the output voltage feedback loop is enabled.

Fig. 15 shows the steady state responses of output voltages (*abc* and *dq* frames) and load currents (*abc* frame) under 5kW resistive load in the case of −30% parameter mismatch obtained with the DB control presented in [7] and SMC presented in [23]. It is obvious that the output voltages obtained with both control methods are sinusoidal. As can be seen from *dq* frame results, both control methods offer good

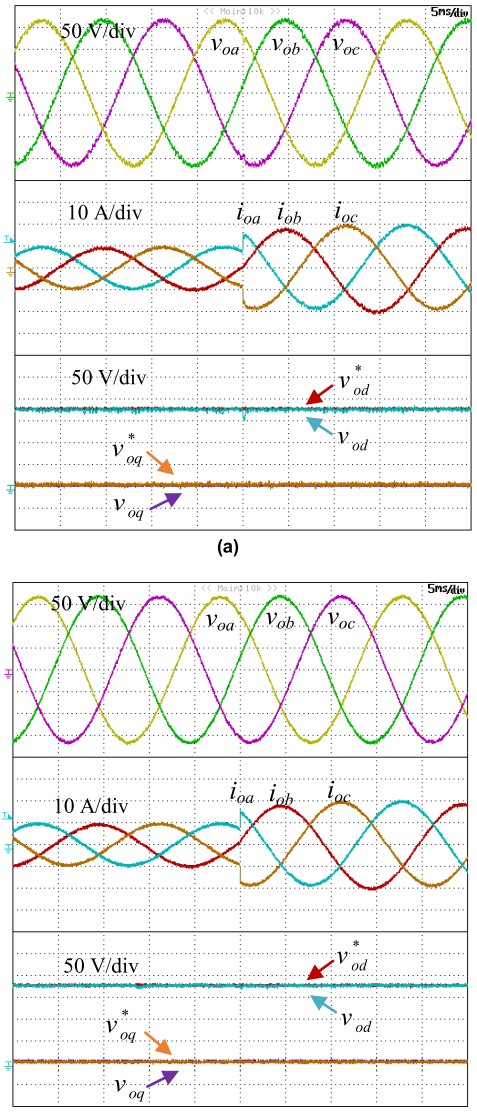

FIGURE 17. Dynamic responses of output voltages (*abc* and *dq* frames) and load currents (*abc* frame) for an abrupt change in linear load from 2.5kW to 5kW in case of −30% parameter mismatch obtained with: (a) DB control, (b) SMC.

tracking performance. Fig. 16 shows harmonic spectrums of output voltage that corresponds to Fig. 15. It is apparent that the output voltage obtained with SMC is less distorted. On the other hand, comparing Fig. 14(a) with Fig. 16, one can easily see that the output voltages under linear load obtained with the proposed method are less distorted. The measured THD values of output voltage obtained with DB and SMC methods are 1.5% and 1.3%, respectively. The 3^{rd} and 5^{th} harmonic components are negligibly small.

Fig. 17 shows the dynamic responses of output voltages and load currents for an abrupt change in the resistive load from 2.5kW to 5kW in the case of −30% parameter mismatch obtained with DB and SMC methods. It is clear that both methods offer good dynamic response and tracking performance. Comparing Fig. 11 and Fig. 17, it can be seen that

TABLE 2. Measured steady-state error and THD values of output voltage under linear and nonlinear loads with various parameter mismatches.

	Output Voltage Loop	Parameter Mismatch	Steady-State Error (Volt)	THD (%)
Linear Load	Enabled	+30%	1	1.2
		0	0	0.9
		-30%	2	1.2
	Disabled	+30%	14	8.6
		0	0	3.8
		-30%	15	8.7
Non-Linear Load	Enabled	+30%	2	2.6
		0	0	2.2
		-30%	1	2.6
	Disabled	+30%	17	9.5
		0	2	4.1
		-30%	17	9.6

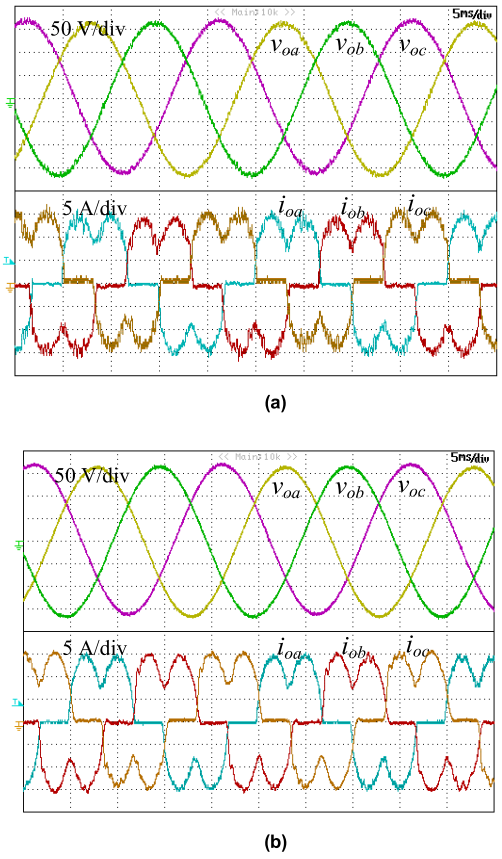

FIGURE 18. Steady-state responses of output voltages and load currents under nonlinear load in case of −30% parameter mismatch obtained with: (a) DB control, (b) SMC.

the dynamic performances of DB, SMC and proposed control methods are close to each other. However, it is worth noting that the major disadvantage of DB control is its sensitivity to parameter variations. On the other hand, SMC method suffers from chattering.

Fig. 18 shows the steady-state responses of the three-phase output voltages and load currents under nonlinear load in the case of −30% parameter mismatch obtained with DB and SMC methods.

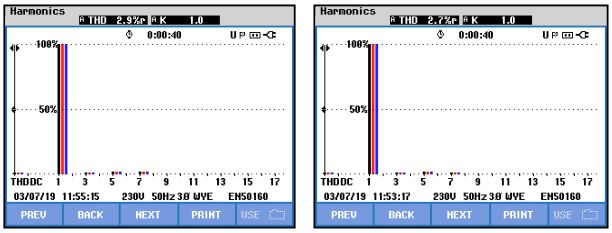

(a) (b)

FIGURE 19. Harmonic spectrums of the output voltage under nonlinear load obtained with: (a) DB control, (b) SMC.

TABLE 3. Measured steady-state error and THD values of output voltage under linear and nonlinear loads obtained with DB and SMC methods in cases of various parameter mismatches.

	Method	Parameter Mismatch	Steady-State Error (Volt)	THD (%)
Linear Load	DB	+30%	5	1.5
		0	2	1.2
		-30%	6	1.5
	SMC	+30%	4	1.4
		0	2	1.1
		-30%	2	1.3
Non-Linear Load	DB	+30%	6	2.9
		0	4	2.5
		-30%	5	2.9
	SMC	+30%	2	2.7
		0	1	2.2
		-30%	3	2.7

Comparing the nonlinear load performances of DB and SMC, it can be seen that the SMC method leads to less distorted output voltages than the DB control. On the other hand, comparing Fig. 13(a) and Fig. 18, the output voltages obtained with the proposed control have better waveform quality.

This fact can be verified in Fig. 19 where harmonic spectrums of output voltage obtained by DB and SMC methods corresponding to Fig. 18 are shown. The measured THD values attained by DB and SMC methods are 2.9% and 2.7%, respectively. The 3^{rd}, 5^{th} and 7^{th} harmonic components are negligibly small. Comparing THD values in Fig. 19 with the THD value in Fig. 14(b), one can easily see that the THD of output voltage under nonlinear load obtained with the proposed method is less than that obtained with the DB and SMC methods under the same load condition.

The measured steady-state error and THD values of the output voltage under linear and nonlinear load types obtained with DB and SMC methods using various parameter mismatch amounts are shown in Table 3. Comparing Table 2 with Table 3, it can be deduced that the proposed control method provides better performance in terms of steady-state error and THD.

VI. CONCLUSION

A Lyapunov-energy-function-based control method with output voltage feedback loops is proposed for three-phase UPS inverters with an output *LC* filter. It is demonstrated that the traditional Lyapunov-energy-function-based control method causes steady-state error and distortion in the output voltage and weak robustness against variations in *LC* filter parameters. Therefore, a Lyapunov-energy-function-based control method with output voltage feedback loops is proposed. It is shown that the proposed control method not only preserves the stability of the inverter, but also reduces the steady-state error in the output voltage considerably, improves the quality of the output voltage and strengthens the robustness against variations in *LC* filter parameters. Inclusion of output voltage feedback loops shifts the dominant closed-loop poles away from the imaginary axis. As a consequence of such movement, the proposed control method offers strong robustness against variations in *LC* filter, high-quality sinusoidal output voltage along with acceptable THD values under linear and nonlinear loads, fast dynamic response under abrupt load changes, and negligible steady-state error in the output voltage. The experimental results show the effectiveness of the proposed control method under linear and nonlinear loads.

REFERENCES

[1] F. Botteron and H. Pinheiro, "A three-phase UPS that complies with the standard IEC 62040-3," *IEEE Trans. Ind. Electron.*, vol. 54, no. 4, pp. 2120–2136, Aug. 2007.

[2] M. Aamir, K. A. Kalwar, and S. Mekhilef, "Review: Uninterruptible power supply (UPS) system," *Renew. Sustain. Energy Rev.*, vol. 58, pp. 1395–1410, May 2016.

[3] P. Cortes, G. Ortiz, J. I. Yuz, J. Rodriguez, S. Vazquez, and L. G. Franquelo, "Model predictive control of an inverter with output *LC* filter for UPS applications," *IEEE Trans. Ind. Electron.*, vol. 56, no. 6, pp. 1875–1883, Jun. 2009.

[4] V. Yaramasu, M. Rivera, M. Narimani, B. Wu, and J. Rodriguez, "Model predictive approach for simple and effective load voltage control of four-leg inverter with an output *LC* filter," *IEEE Trans. Ind. Electron.*, vol. 61, no. 10, pp. 5259–5270, Oct. 2014.

[5] H. T. Nguyen, J. Kim, and J. W. Jung, "Improved model predictive control by robust prediction and stability-constrained finite states for three-phase inverters with an output *LC* filter," *IEEE Access*, vol. 7, pp. 12673–12685, 2019.

[6] P. Mattavelli, "An improved deadbeat control for UPS using disturbance observers," *IEEE Trans. Ind. Electron.*, vol. 52, no. 1, pp. 206–211, Feb. 2005.

[7] M. Pichan, H. Rastegar, and M. Monfared, "Deadbeat control of the stand-alone four-leg inverter considering the effect of the neutral line inductor," *IEEE Trans. Ind. Electron.*, vol. 64, no. 4, pp. 2592–2601, Apr. 2017.

[8] G. Escobar, A. A. Valdez, J. Leyva-Ramos, and P. Mattavelli, "Repetitive-based controller for a UPS inverter to compensate unbalance and harmonic distortion," *IEEE Trans. Ind. Electron.*, vol. 54, no. 1, pp. 504–510, Feb. 2007.

[9] S. Jiang, D. Cao, Y. Li, J. Liu, and F. Z. Peng, "Low-THD, fast-transient, and cost-effective synchronous-frame repetitive controller for three-phase UPS inverters," *IEEE Trans. Power Electron.*, vol. 27, no. 6, pp. 2994–3005, Jun. 2012.

[10] N. Marati and D. Prasad, "A modified feedback scheme suitable for repetitive control of inverter with nonlinear load," *IEEE Trans. Power Electron.*, vol. 33, no. 3, pp. 2588–2600, Mar. 2018.

[11] Z. Liu, B. Zhang, K. Zhou, and J. Wang, "Virtual variables sampling discrete Fourier transform based selective odd-order harmonic repetitive control of DC/AC converters," *IEEE Trans. Power Electron.*, vol. 33, no. 7, pp. 6444–6452, Jul. 2018.

[12] Y. Ye, G. Xu, Y. Wu, and Q. Zhao, "Optimized switching repetitive control of CVCF PWM inverters," *IEEE Trans. Power Electron.*, vol. 33, no. 7, pp. 6238–6247, Jul. 2018.

[13] G. Willmann, D. F. Coutinho, L. F. A. Pereira, and F. B. Libano, "Multi-loop H-infinity control design for uninterruptible power supplies," *IEEE Trans. Ind. Electron.*, vol. 54, no. 3, pp. 1591–1602, Jun. 2007.

[14] D.-E. Kim and D.-C. Lee, "Feedback linearization control of three-phase UPS inverter systems," *IEEE Trans. Ind. Electron.*, vol. 57, no. 3, pp. 963–968, Mar. 2010.
[15] A. Houari, H. Renaudineau, J. P. Martin, S. Pierfederici, and F. M. Tabar, "Flatness-based control of three-phase inverter with output *LC* filter," *IEEE Trans. Ind. Electron.*, vol. 59, no. 7, pp. 2890–2897, Jul. 2012.
[16] T. D. Do, V. Q. Leu, Y. S. Choi, H. H. Choi, and J. W. Jung, "An adaptive voltage control strategy of three-phase inverter for stand-alone distributed generation systems," *IEEE Trans. Ind. Electron.*, vol. 60, no. 12, pp. 5660–5672, Dec. 2013.
[17] B. Tamyurek, "A high-performance SPWM controller for three-phase ups systems operating under highly nonlinear loads," *IEEE Trans. Power Electron.*, vol. 28, no. 8, pp. 3689–3701, Aug. 2013.
[18] H. Deng, R. Oruganti, and D. Srinivasan, "Analysis and design of iterative learning control strategies for UPS inverters," *IEEE Trans. Ind. Electron.*, vol. 54, no. 3, pp. 1739–1751, Jun. 2007.
[19] J. S. Lim, C. Park, J. Han, and Y. I. Lee, "Robust tracking control of a three-phase DC-AC inverter for UPS applications," *IEEE Trans. Ind. Electron.*, vol. 61, no. 8, pp. 4142–4151, Aug. 2014.
[20] E.-K. Kim, F. Mwasilu, H. H. Choi, and J.-W. Jung, "An observer-based optimal voltage control scheme for three-phase UPS systems," *IEEE Trans. Ind. Electron.*, vol. 62, no. 4, pp. 2073–2081, Apr. 2015.
[21] O. Kukrer, H. Komurcugil, and A. Doganalp, "A three-level hysteresis function approach to the sliding mode control of single-phase UPS inverters," *IEEE Trans. Ind. Electron.*, vol. 56, no. 9, pp. 3477–3486, Sep. 2009.
[22] H. Komurcugil, "Rotating-sliding-line-based sliding-mode control for single-phase ups inverters," *IEEE Trans. Ind. Electron.*, vol. 59, no. 10, pp. 3719–3726, Oct. 2012.
[23] M. Pichan and H. Rastegar, "Sliding-mode control of four-leg inverter with fixed switching frequency for uninterruptible power supply applications," *IEEE Trans. Ind. Electron.*, vol. 64, no. 8, pp. 6805–6814, Aug. 2017.
[24] H.-S. Kim, H.-S. Jung, and S.-K. Sul, "Discrete-time voltage controller for voltage source converters with *LC* filter based on state-space models," *IEEE Trans. Ind. Appl.*, vol. 55, no. 1, pp. 529–540, Jan./Feb. 2019.
[25] H. Komurcugil and O. Kukrer, "Lyapunov-based control for three-phase PWM AC/DC voltage-source converters," *IEEE Trans. Power Electron.*, vol. 13, no. 5, pp. 801–813, Sep. 1998.
[26] S. Rahmani, A. Hamadi, and K. Al-Haddad, "A Lyapunov-function-based control for a three-phase shunt hybrid active filter," *IEEE Trans. Ind. Electron.*, vol. 59, no. 3, pp. 1418–1429, Mar. 2012.
[27] R. J. Minnichelli, J. J. Anagnost, and C. A. Desoer, "An elementary proof of Kharitonov's stability theorem with extensions," *IEEE Trans. Autom. Control*, vol. 34, no. 9, pp. 995–998, Sep. 1989.
[28] B. Basile and M. K. Pachipulusu, "10-kW, three-level, three-phase grid tie inverter reference design for solar string inverters," TI Designs, Dallas, TX, USA, Tech. Rep. TIDA 01606, 2018, pp. 1–37.

SERTAC BAYHAN (M'14–SM'18) received the bachelor's, M.Sc., and Ph.D. degrees in electrical engineering from Gazi University, Ankara, Turkey, in 2006, 2008, and 2012, respectively, and graduated as a Valedictorian. In 2008, he joined the Electronics and Automation Engineering Department, Gazi University, as a Lecturer, where he was promoted to an Assistant Professor and an Associate Professor, in 2013 and 2017, respectively. From 2014 to 2018, he was also with Texas A&M University at Qatar as an Associate Research Scientist. He is currently with the Qatar Environment and Energy Research Institute (QEERI) as a Scientist.

He has authored 130 high-impact journals and conference papers. He has coauthored two books and three book chapters. His research interests include advanced control of PV systems, microgrids, and smart grid applications. He has led multi-PI projects with collaborators from all over the world. Because of the visibility of his research, he has been recently elected as a Chair of IES Power Electronics Technical Committee and selected as a Co-Chair of the IEEE-IES Student and Young Professional Activities Program. He currently serves as an Associate Editor for the IEEE TRANSACTIONS ON INDUSTRIAL ELECTRONICS and a Guest Editor for the IEEE TRANSACTIONS ON INDUSTRIAL INFORMATICS.

S. SAJJAD SEYEDALIPOUR received the B.Sc. degree from the University of Zanjan, Zanjan, Iran, in 2009, and the M.Sc. degree from the K. N. Toosi University of Technology, Tehran, Iran, in 2012, both in electrical engineering.

His current research interests include control of power converters, active power filters, and distributed generation systems.

HASAN KOMURCUGIL (S'94–M'99–SM'12) received the B.Sc., M.Sc., and Ph.D. degrees in electrical engineering from Eastern Mediterranean University (EMU), Famagusta, North Cyprus, Turkey, in 1989, 1991, and 1998, respectively, where he joined the Computer Engineering Department, in 1998, as an Assistant Professor, and was promoted to an Associate Professor and a Professor in 2002 and 2008, respectively. From 2004 to 2010, he was the Head of the Computer Engineering Department, EMU. In 2010, he played an active role in preparing the department's first self-study report for the use of Accreditation Board for Engineering and Technology. From 2010 to 2019, he served as the Board Member for the Higher Education, Planning, Evaluation, Accreditation and Coordination Council (YODAK), North Cyprus. He is currently a full-time Professor with the Computer Engineering Department, EMU. His research interests include power electronics and innovative control methods for power converters. He was a recipient of the Best Presentation Recognitions at the 41st and 42nd Annual Conferences of the IEEE Industrial Electronics Society, in 2015 and 2016, respectively. He was a corresponding Guest Associate Editor for Emerging Electric Machines and Drives for Smart Energy Conversion in the IEEE TRANSACTIONS ON ENERGY CONVERSION. He is currently a Guest Editor for Identification and Observation Informatics for Energy Generation, Conversion, and Applications and Recent Advances on Sliding Mode Control and Its Applications in Modern Industrial Systems in the IEEE TRANSACTIONS ON INDUSTRIAL INFORMATICS. He is also an Associate Editor of the IEEE TRANSACTIONS ON INDUSTRIAL ELECTRONICS and the IEEE TRANSACTIONS ON INDUSTRIAL INFORMATICS.

HAITHAM ABU-RUB (M'99–SM'07–F'18) received the M.Sc. degree in electrical engineering from the Gdynia Marine Academy, Gdynia, Poland, in 1990, and the Ph.D. degree from the Gdansk University of Technology, Gdansk, in 1995. Since 2006, he has been with the Texas A&M University at Qatar, Doha, Qatar, where he is currently a Professor, the Chair of the Electrical and Computer Engineering Program, and the Managing Director of the Smart Grid Center Extension. He has authored more than 300 journals and conference papers and has earned and supervised many research projects. He is currently leading many projects on photovoltaic and hybrid renewable power generation systems with different types of converters and electric drives. He has coauthored four books, two of which are published by Wiley. He has also authored or coauthored five book chapters. His research interests include energy conversion systems, including electric drives, power electronic converters, renewable energy, and smart grid. He received many prestigious international awards, such as the American Fulbright Scholarship, the German Alexander von Humboldt Fellowship, the German DAAD Scholarship, and the British Royal Society Scholarship. He is also an Editor of several IEEE journals.